A combinatorial study of SiGeAsTe thin films for application as an Ovonic threshold switch selector

Wouter Devulder[a], Daniele Garbin[a], Sergiu Clima[a], Gabriele Luca Donadio[a], Andrea Fantini[a], Bogdan Govoreanu[a], Christophe Detavernier[b], Larry Chen[c], Michael Miller[c], Ludovic Goux[a], Sven Van Elshocht[a], Johan Swerts[a], Romain Delhougne[a], Gouri Sankar Kar[a]

[a] *IMEC, Kapeldreef 75, Leuven, 3001, Belgium*
[b] *Ghent University, Dept. of Solid State Sciences, Krijgslaan, Ghent, 9000, Belgium*
[c] *Intermolecular Inc. is a subsidiary of Merck KGaA, Darmstadt, Germany, 3011 North First Street, San Jose, CA 95134, CA 95134, USA*

Abstract

In this paper, we investigate the thermal stability of a wide range of ternary and quaternary (Si)GeAsTe alloy thin films. These type of materials are reported to show Ovonic threshold switching, which means they conduct the current above a specific threshold voltage and are not conducting at lower voltages, making them ideal as a selector element for crosspoint memory devices. For threshold switching to occur in these chalcogenides, the amorphous state of the material is crucial, and hence the material may not crystallize below 400°C to be compatible with temperatures used in device process flows. A combinatorial deposition technique is used to create a thin film library of 36 different compositions, and *in situ* X-ray diffraction and X-ray fluorescence spectroscopy is used to investigate the thermal stability of the films. We show that Si doping of GeAsTe improves the thermal stability by increasing the crystallization temperature and small amounts of Si (i.e. 5 at%) decreases the tendency to lose material by sublimation. Also capping the films with a W cap avoids material loss if the capping layer does not show cracking under annealing. An optimal chalcogenide composition, being $As_{50}Te_{20}Ge_{20}Si_{10}$ combined with a W electrode is identified and is integrated in 65 nm mushroom type devices for electrical characterization. The material shows threshold switching and excellent endurance with over 10^8 cycles.

Keywords: Chalcogenides, thermal stability, *in situ* X-ray diffraction, Ovonic threshold switching, selectors

1. Introduction

Chalcogenides are materials with at least one of the elements S, Se or Te. This covers a wide range of materials with many different properties and applications, ranging from (2D) transition metal dichalcogenides [1], to thin film

Email address: Wouter.Devulder@imec.be (Wouter Devulder)

solar cell materials [2] and chalcogenide glasses for application in optics [3, 4] and emerging memory technologies [5]. For the latter, they are of interest for application in storage class memory (SCM), which fills the gap in the memory hierarchy between non-volatile Flash and volatile dynamic random access memory [5]. Phase change memory (PCM) has been demonstrated to be a good candidate for SCM, where typically $Ge_2Sb_2Te_5$ or a modification thereof is used [6]. The memory state is achieved here by switching the material between a crystalline and amorphous state, which have a different electrical resistivity. In order to integrate these memory cells in dense cross point memory arrays, a two-terminal selector device is necessary to eliminate sneak path currents [7]. A selector device is a component in series with the memory element that only conducts the current above a specific threshold voltage V_t. In this way, when a read voltage is applied on a specific cell, the unaddressed cells that feel a voltage $V_{read}/2$ and are in a low resistive state will not conduct current as the selector element prevents this. Several chalcogenides are reported to show threshold switching, referred to as *Ovonic threshold switching* (OTS) [8], and this makes them attractive for application as a selector.

Different chalcogenides have been investigated and reported for selector applications, starting from binary systems like Si-Te [9, 10], Ge-Te [11], Zn-Te [12], Ge-Se [13, 14] to more complex ternary and quaternary systems like Si-As-Te [15, 16] and Si-Ge-As-Te [17]. The materials are often further doped [18, 19, 20, 21] to improve device performance and materials stability [22, 23].

It is challenging to find a material which shows the required electrical behavior and good thermal stability. From device perspective, the material should have a low leakage current at 1/2 V_t (i.e. the voltage that may be present over a non-address cell), have a high switching speed, high endurance (i.e. $> 10^8$ cycles) and allow a high current density ($> 10\,\mathrm{MA/cm^2}$) in the on state, compatible with the memory device. To be compatible with integration flows in semiconductor processing, the material should have a sufficiently high thermal stability to withstand back end of line (BEOL) processing, where it should withstand temperatures up to 450°C for 30 min [5]. To be functional as OTS, the chalcogenide should remain in the amorphous state, and hence should not crystallize up to these temperatures.

In this work, we conduct a thorough material screening of a large set of ternary and quaternary (Si-)Ge-As-Te compositions. The compositions under study are selected after careful literature review of reported bulk phase diagrams and models to predict the thermal stability and expected OTS behavior. The selected composition range is then deposited in 20 nm thin films where we make use of a combinatorial deposition technique. The thermal stability is investigated, where we determine the crystallization temperature and verify the film and stack integrity after anneal. A thermally stable composition is selected from this study, and is integrated in mushroom type devices with a 65 nm bottom electrode contact for characterization of the threshold switching behavior. A high endurance OTS selector with over 10^8 cycles is demonstrated. Furthermore, ab initio simulations are carried out to understand the electronic structure of the material and to explain its threshold switching properties.

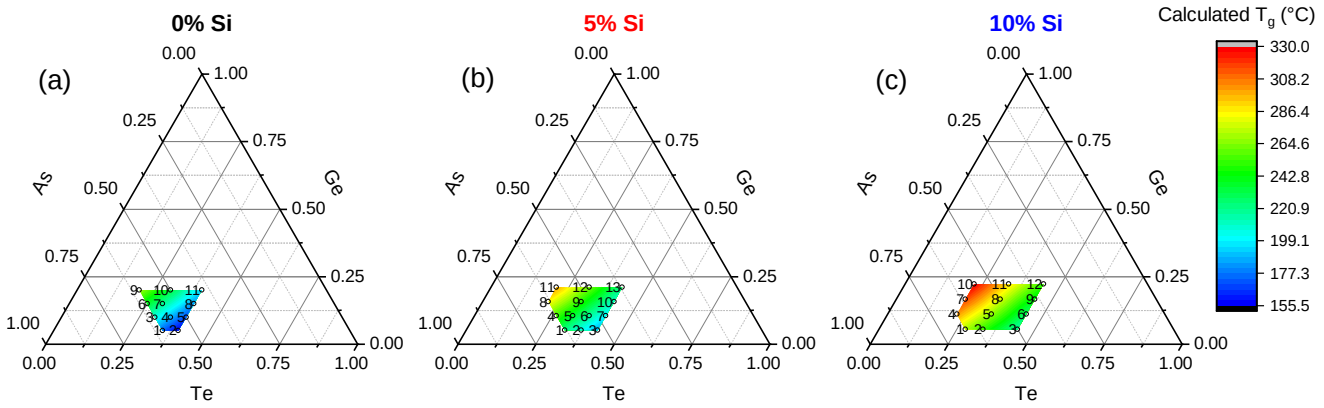

Figure 1: Compositions under study, depicted in the ternary Ge-As-Te composition space. (a) Ternary Ge-As-Te, (b) Si-Ge-As-Te with 5 at% Si and (c) with 10 at% Si. The quaternary systems (b) and (c) are projected on the Ge-As-Te plane for ease of comparison. The color code indicates the glass transition temperature, calculate using the Lankhorst model.

2. Experimental Procedures

A set of 36 different compositions have been identified and are deposited by co-sputtering from $Ge_5As_{75}Te_{20}$, Ge, Si and As_2Te_3 sputter targets. The composition of the films was varied by adapting the power applied on the different targets. The compositions are depicted in the ternary Ge-As-Te diagram in Figure 1, and the motivation for these compositions will be further explained in the Theory section. Three main groups of compounds have been prepared: (i) ternary Ge-As-Te (Figure 1a), (ii) quaternary Si-Ge-As-Te containing 5 at% Si (Figure 1b) and (iii) quaternary films with 10 at% Si (Figure 1c). For the quaternary systems, the points are projected in the ternary Ge-As-Te plane for ease of comparison. Every compound is numbered in the figure, and we will further refer to the compositions in symbolic notation x%Si_(compound nr.) (e.g. 5%Si_10 is then a quaternary film with 5 % Si, index 10, which has a composition of 5 % Si, 40 % As, 15 % Ge and 40 % Te). The compositions have been verified by means of Rutherford backscattering spectroscopy (RBS) and wavelength dispersive X-ray fluorescence spectroscopy (WD-XRF). A summary of the prepared compounds with their labeling and measured compositions is given in the Supporting Information Table S1. The chalcogenide films are deposited in 24 mm diameter spots on a 300 mm wafer. The Si wafer has a 300 nm SiO_2 thermal oxide on top. The chalcogenide layer is 20 nm thin and is covered in situ with a 30 nm W cap to avoid evaporation of the films during annealing. Meanwhile, W is a valid top electrode for use in a device stack. In this way, the thermal stability of a device compatible material stack is investigated.

The crystallization behavior of the films is investigated by means of *in situ* X-ray diffraction (XRD). A Bruker D8 Discover diffractometer is equipped with

a Cu K_α X-ray source, a linear detector and a home built annealing chamber [24]. The source and detector are fixed to a specific θ-2θ position, and by means of the linear detector, a fixed 2θ window of 20° is monitored during anneal. For our measurements, the source and detector are fixed to 14 and 28° respectively, measuring the 2θ window $18 - 38°$. The samples are annealed at a constant heating rate of 0.2°C/s in He atmosphere and at the same time, XRD patterns are collected with a collection time of 5 s. In this way, an *in situ* XRD pattern is measured with a resolution of 1°C. Crystallization of the films is then detected by the appearance of diffraction peaks. Moreover, identification of the diffraction peaks allows us to identify the different compounds that crystallize and their crystallographic structure.

Energy dispersive X-ray fluorescence spectroscopy (XRF) was used to verify if any material was lost after annealing [25]. Any loss of material is detected as a decrease in intensity of the characteristic fluorescent peaks of the elements (Ge, As and Te) after anneal, compared to the as-deposited film. The stack integrity and surface morphology was investigated by optical microscopy and scanning electron microscopy (SEM).

An optimal chalcogenide composition in terms of materials stability was identified and the selected compostion is deposited in a set of 24 mm diameter spots, aligned on the dies of a 300 mm device wafer. The chalcogenide is patterned by ion beam etch to create a mushroom type of device, where the bottom electrode is a TiN plug with a diameter of 65 nm. The devices were characterized in AC mode using an Agilent 81110A pulse generator and a LeCroy WavePro735Zi oscilloscope. Low current measurements were carried out using a Keithley K2602A source measure unit. The current through the devices is limited by a varying on chip series resistor.

Ab initio simulations have been carried out to get an understanding of the electronic structure of the material to explain the switching properties of the material. Density Function Theory (DFT) simulations were performed on 10 different models that were generated with a melt-and-quench technique (see reference [26] to previous work for more details on the computational details). The electronic structures were assessed by using a hybrid exchange-correlation functional (HSE), combining GTH pseudopotentials and DZVP basis sets in CP2K [27]. The valence and conduction edges were found by applying a threshold on Inverse Participation Ratio (IPR) coefficients, computed for each state of the amorphous model.

3. Theory

To be compatible with BEOL processing, the OTS material should withstand temperatures up to at least 400°C, meaning that it should not melt and evaporate, nor sublimate, and the stack needs to remain intact (i.e. no surface morphology degradation or layer intermixing) up to this temperature.

Although we are interested in thin films, the bulk properties of Ge-As-Te are a good starting point to select the compositions where a good thermal stability can be expected. Figure 2a gives an overview - without claiming to be complete

- of the intermetallic compounds that are reported, both binary and ternary, and their corresponding melting temperature (T_m). For other compositions, phase separation and hence co-existence of more phases is expected in the crystalline state. On the pseudo-binary As_2Te_3-GeTe line [28, 29], the intermetallic compound family $Ge_nAs_2Te_{3+n}$ (with n an integer number) can be found. As_2Te_3 melts at 385°C, and upon adding GeTe, a eutectic point (indicated as E in the figure) with a lower melting temperature (370°C) is present. Upon moving further to the GeTe rich side, the $Ge_nAs_2Te_{3+n}$ compounds are formed. Those with n from 1 to 4 are formed peritectically, with the temperature indicated as T_p. Hence upon heating these compounds, a solid and liquid is formed above T_p. For all these phases this is above 400°C and hence thermal stability is better. At the Te rich side of the binary As-Te and Ge-Te system, eutectic points with melting temperatures below 400°C are present. Hence this Te rich sub triangle (orange shaded region in Figure 2a) is to be avoided because of these low melting temperatures, and we select more As and Ge rich compositions.

Figure 2a also indicates other reported cross sections [28, 29, 30, 31, 32], on which we marked the points where an invariant reaction ($U_{1,2}$) involving a liquid phase [33] occurs. This is at relative high temperature, and hence the As rich side of As-Te, where Ge is added forms the starting point for our materials exploration. The compositions under study, are projected in the ternary Ge-As-Te and shown in Figure2a.

For OTS applications, the chalcogenide should stay in the amorphous phase, hence it should have a good resistance against crystallization. To get a better understanding of the impact of composition on crystallization temperature, the glass transition temperature T_g was calculated for the alloys under study, by means of the model proposed by Lankhorst [34]. This model makes use of a semi-empirical formula that links the glass forming temperature to the average bond strength. The latter is calculated from the bond strengths between the different elements (see Table S2 in the Supporting Information) and the number of these bonds that are formed. Because the glass transition temperature is a lower limit for the crystallization temperature T_x, the stability of the alloys against crystallization can be estimated [34, 35]. Figure 1a, shows T_g of the ternary Ge-As-Te compositions. We see that T_g is the lowest for Ge poor and Te rich compositions and increases when more As and/or Ge is added. When Si is added (5 at% and 10 at% in Figures 1b and c respectively), T_g increases further. This is because addition of these elements add more and strong bonds to the system, increasing T_g. Because T_g is a lower limit for T_x, a similar trend is to be expected for the crystallization temperature. This makes sense because when more strong bonds are present, atomic rearrangements that are necessary for crystallization to proceed will be more difficult, hence T_x will increase.

The final goal is to obtain a thermally stable material that shows OTS behavior, for application as selector. To assess the probability that these materials may show threshold switching, the compositions are plotted in the r_π^{-1}-r_σ map (Figure 2b), as was proposed by Velea et al. [22]. The coordinates r_σ and r_π^{-1} are a measure for the ionicity and covalency respectively of the bonds. The map is an extension of the original map for phase change materials [36] with an

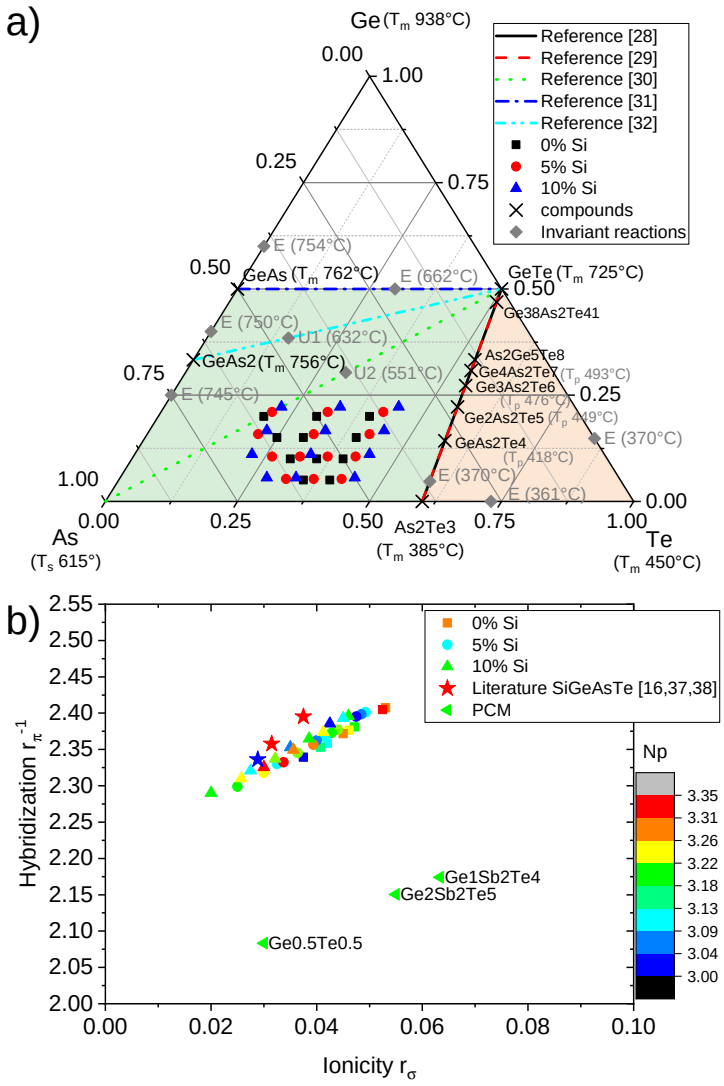

Figure 2: (a) Ternary Ge-As-Te composition space, indicating the intermetallic binary and ternary compounds with their melting temperature (T_m) or temperature where they are formed peritectically (T_p). The reported ternary cross sections are also indicated, together with the invariant reactions deduced from these diagrams. The compositions that are studied in this work are projected in the Ge-As-Te composition diagram. (b) Compositions under study plotted in the r_π^{-1}-r_σ map. A few reported SiGeAsTe compositions that show OTS are plotted as well, together with a few reference PCM materials. The number of average p-electrons (N_p) is plotted as a color map.

average number of p-electrons equal to 3. Velea et al. [22] noticed that the OTS materials group together towards larger r_{π}^{-1}, meaning a higher hybridization tendency and a more covalent nature of the bonds compared to phase change materials. Note that the average number of p-electrons is also slightly deviating from 3 (which was fixed in the original PCM map), and that's why this is added as a third parameter, shown as color map in Figure 2b. A few other SiGeAsTe alloys that are reported to show OTS behavior [16, 37, 38] are also depicted, together with some reference PCM materials to illustrate the different locations of these materials in the map. It is clear that the compositions under study lay in the region of OTS materials, giving confidence of their OTS functionality.

4. Results and discussion

4.1. Thermal stability study

The thermal stability was investigated by means of *in situ* XRD. In a first step, the annealing temperature was limited to 450°C, to avoid material loss because of sublimation or evaporation. No crystallization could be observed for any of the 36 compounds. All samples were subjected to XRF before and after anneal, and integrated peak intensities of As and Te were compared before and after anneal. The ratio of the integrated intensity of the characteristic line after anneal, and the intensity of a reference sample before anneal (I/I_0) is plotted in Figure 3 for both As and Te. The ratio should be equal to 1 if no material loss occurred, and less then 1 if material was lost by annealing. The error bars indicate the absolute error originating from the counting statistical error from the XRF counts. Note that a few points have a value larger than 1 (even taking the error bar into account), which is unphysical as no material can be added after anneal. However, this is explained by the fact that the reference sample before anneal is not exactly the same piece of sample as the one that is annealed. Hence a small fluctuation in thickness or composition explains this deviation and causes an additional error on this ratio. However, despite this effect, it is clear that the ternary Ge-As-Te samples are more prone to As loss. Indeed, the intensity ratio of As is between 50 and 85 % (see Figure 3a), whereas for the Si doped films (Figures 3b and c) the As (and Te) ratio is very close to one. Mainly the GeAsTe films with high As and low Ge contents are prone to As loss.

It is clear that Si doping has a positive effect in terms of stability against material loss, and for that reason, the ternary materials are considered less thermally stable and are not further investigated up to higher temperatures, because even more As loss is expected. This was confirmed for one ternary sample with a relative low amount of As (i.e. 0%Si_11) that was annealed to 500°C. This resulted in complete disappearance of As after anneal, only Ge and Te could be detected afterwards. The *in situ* XRD plot is shown in Figure 4a. Diffraction peaks of the rhombohedral GeTe phase show up starting at 467°C, while no traces of As or As containing phases are detected, in agreement with the observed As loss. The way of extracting the crystallization temperature from the *in situ* XRD is illustrated in Figure 4b.

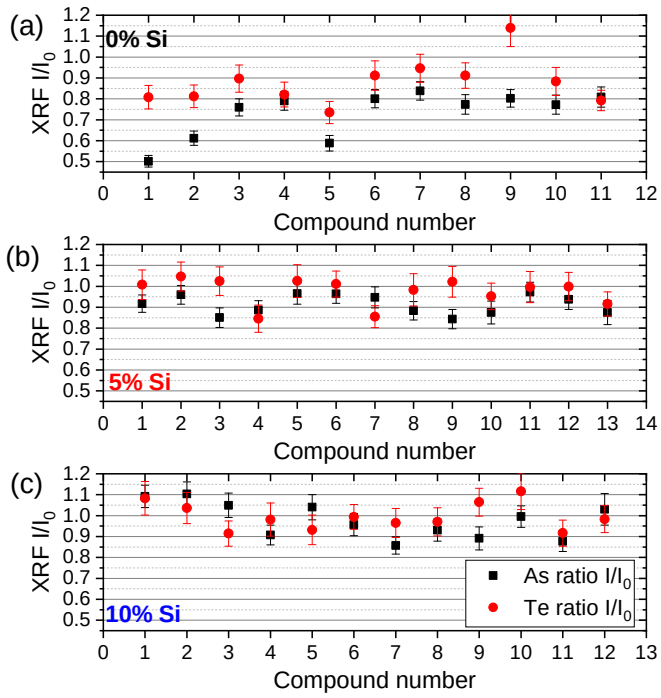

Figure 3: For both As and Te, the ratio of the integrated intensity of their characteristic lines after anneal at 450°C and before anneal is plotted. (a) Ratios for the ternary Ge-As-Te compounds, (b) ratios for the quaternary Si-Ge-As-Te compounds with 5 at% Si and (c) 10 at% Si. The characteristic lines measured are As Kα and Te Lα.

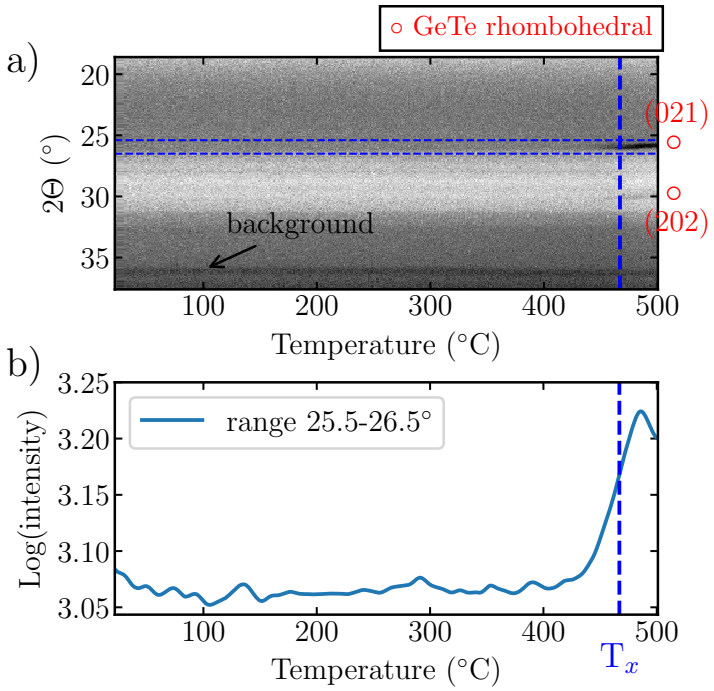

Figure 4: (a) *In situ* XRD plot of the ternary GeAsTe sample 0%Si_11 up to 500°C. The logarithm of the XRD intensity is plotted as a grey scale color map, the y-axis shows the 2θ value and the x-axis the temperature. The diffraction peaks that appear can be assigned to rhombohedral GeTe. The peak at 36° is a background signal. (b) Extraction of the crystallization temperature from the *in situ XRD* measurement. The XRD intensity is integrated in the 2θ range where the diffraction peak of a specific phase occurs (in this case 25.5-26.5° for the (021) peak of rhombohedral GeTe). The crystallization temperature is then defined as the temperature where the maximum change in integrated intensity occurs. In this case, T_x is 467°C.

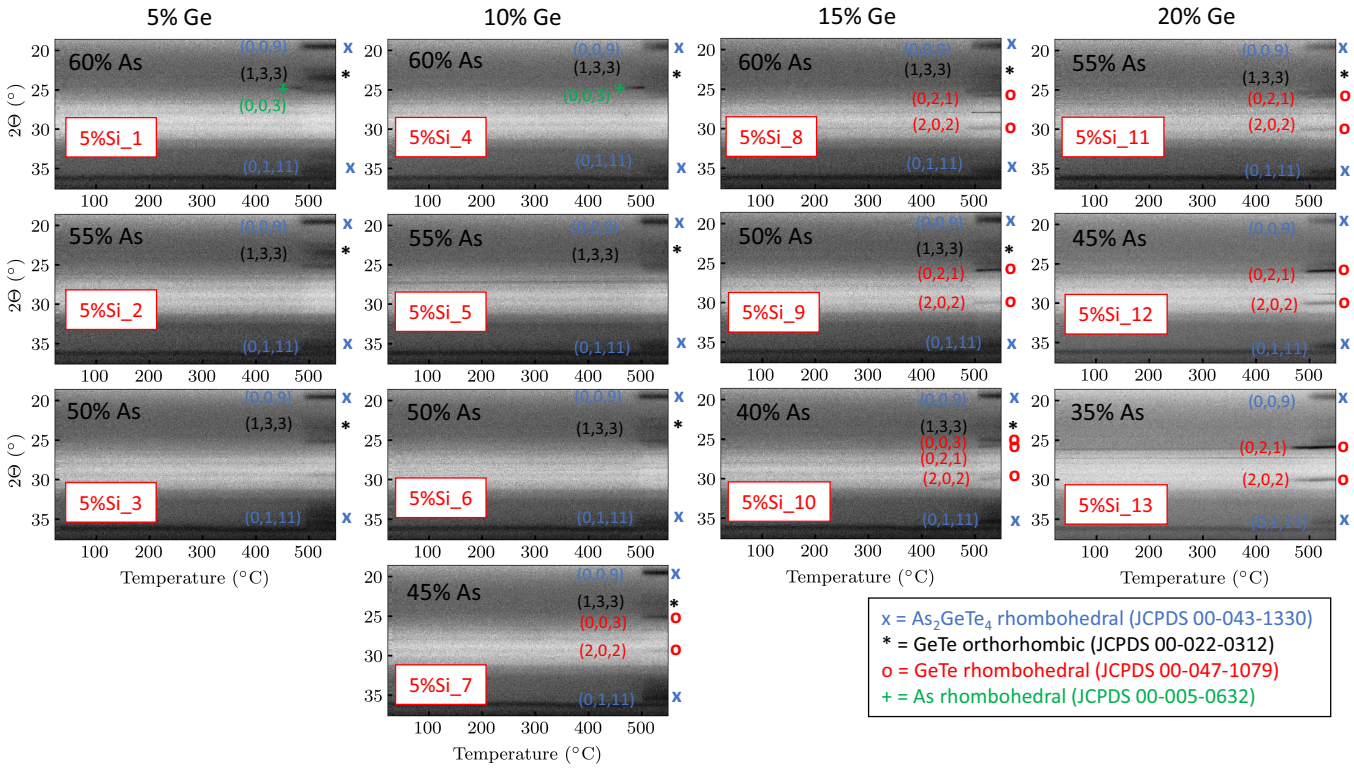

Figure 5: *In situ* XRD measurements of the W capped SiGeAsTe thin films with 5 at% Si. The logarithm of the XRD intensity is plotted as a grey scale color map, the y-axis shows the 2θ value and the x-axis the actual temperature. The observed diffraction peaks are identified and labeled.

The Si doped samples are annealed up to 550°C to induce crystallization and to extract T_x. Figure 5 shows all the *in situ* XRD patterns for the SiGeAsTe samples with 5 at% Si, and the diffraction peaks that appear are identified with the in literature available powder diffraction patterns. The temperature at which a specific phase crystallizes is summarized in Figure 6a, and the temperature range where the phase is present is shaded. For As rich compositions with low amounts of Ge (e.g. 5%Si_1 and 4), a faint peak of rhombohedral As [39] shows up initially, and disappears when rhombohedral As_2GeTe_4 [40] crystallizes. For all compositions, diffraction peaks that can be matched to rhombohedral As_2GeTe_4 appear. Compositions 5%Si_1 and 2 have a clear peak at 23.5° that can be related to the (1,3,3) peak of orthorhombic GeTe [41]. For the others, this peak is rather broad, suggesting an amorphous or nanocrystalline material. For completeness, the appearance of this broad peak is also added to Figure 6a. However, to extract the crystallization temperature for those alloys, it is better to look at the appearance of As or As_2GeTe_4 diffraction peaks. For the films with more Ge (i.e. from sample 5%Si_7 on), diffraction peaks that

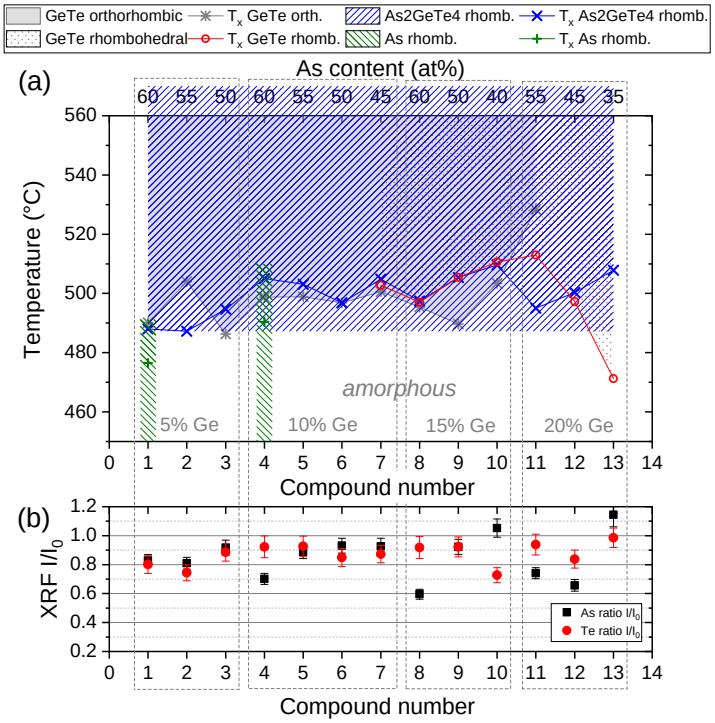

Figure 6: (a) Summary of the crystallization temperatures T_x of the different crystallographic phases for all the SiGeAsTe compounds with 5 at% Si. The temperature region where they are observed is shaded. (b) XRF of the As and Te ratio after and before anneal up to 550°C.

can be matched to rhombohedral GeTe [42] are observed. XRF analysis of the samples after anneal (see Figure 6b) show that the composition is still fairly maintained for most samples. Comparing the extracted T_x with the calculated T_g (see Figure 1), we see that T_x is indeed higher than T_g, however, the change of T_x as function of composition is not so pronounced (only small changes in T_x). The effect may be more clear when a larger spread in composition would be explored.

The same measurements and analysis are carried out for the SiGeAsTe compositions with 10 at% Si. The *in situ* XRD patterns are shown in Figure 7, the identified crystallographic phases are summarized in Figure 8a and the XRF before and after anneal is shown in Figure 8b. The diffraction peaks that appear are very similar to the previous analysis for the compositions with 5 at% Si. However, there are some differences. Comparing the XRF results in Figures 6b and 8b, it is apparent that the As rich compositions with 10 at% Si are more prone to As (and Te) loss compared to the compositions with 5 at% Si. We think that this is caused by phase separation of As and Si when higher Si contents are used. The As-Si bond is a strong bond (see table S2 in the supporting

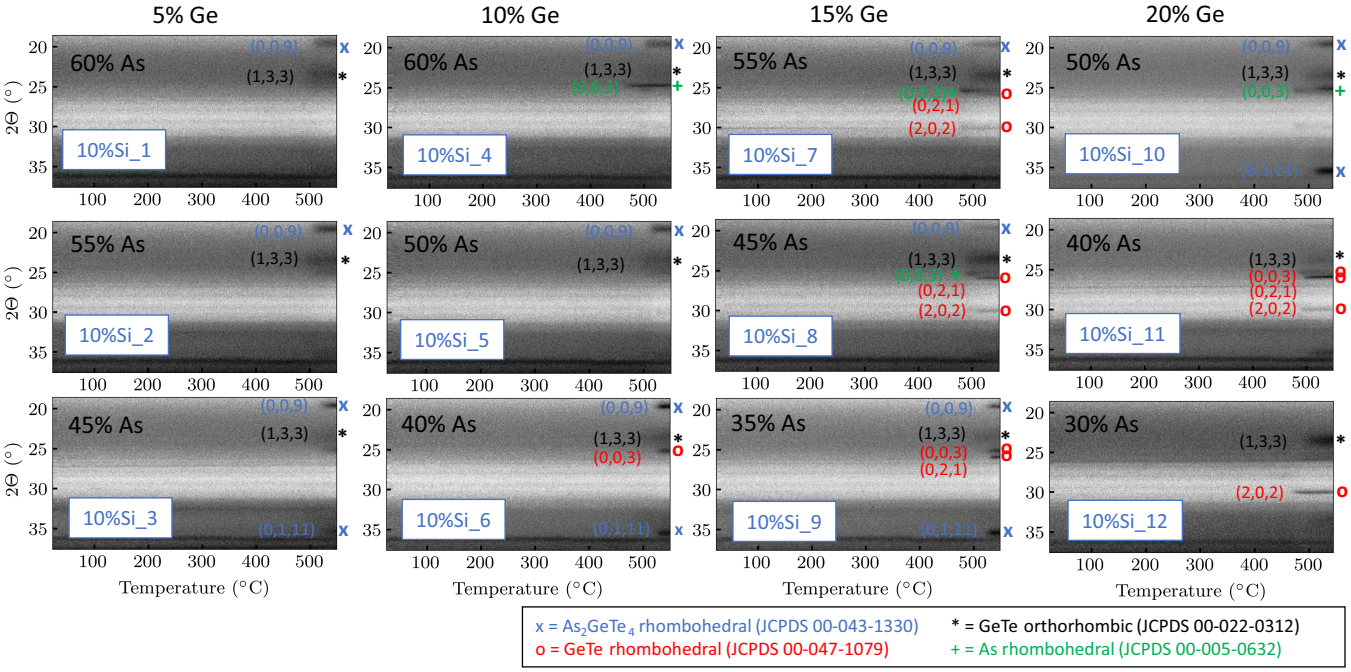

Figure 7: *In situ* XRD measurements of the W capped SiGeAsTe thin films with 10 at% Si. The logarithm of the XRD intensity is plotted as a grey scale color map, the y-axis shows the 2θ value and the x-axis the actual temperature. The observed diffraction peaks are identified and labeled.

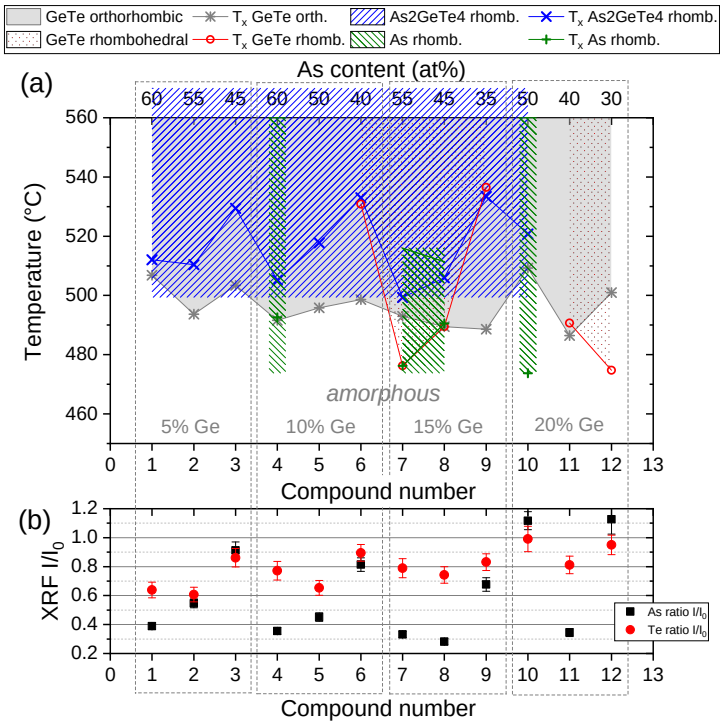

Figure 8: (a) Summary of the crystallization temperatures T_x of the different crystallographic phases for all the SiGeAsTe compounds with 10 at% Si. The temperature region where they are observed is shaded. (b) XRF of the As and Te ratio after and before anneal up to 550°C.

information for theoretical bond strengths), but Si-Si bonds are stronger and may be preferred when more Si is present, leaving more room for pure As, which is then more prone to sublimation. This behavior can be seen in Figure 7, in the *in situ* XRD pattern of composition 10%Si_7: initially rhombohedral As crystallizes, and its diffraction peak disappears upon further heating. This may be caused by consumption of the As when As_2GeTe_4 crystallizes, but maybe also because of As sublimation. Note that the As_2GeTe_4 peak is also not so intense compared to GeTe, because of the low amount of As left. If we compare the T_x of the samples with 5 versus 10 at% Si where no major composition changes occurred, it is clear that T_x is slightly higher, especially for As_2GeTe_4. This can be understood by the Si making strong bonds with the other elements, or by Si chains that make restructuring of the material and hence crystallization more difficult. A broad peak of orthorhombic GeTe shows up again, which points to an amorphous or nanocrystalline nature. The onset of this seems to be less impacted by Si.

There is one As-rich film that does not suffer from this As loss, i.e. 10%Si_10 which has a composition of $As_{50}Te_{20}Ge_{20}Si_{10}$. Here we see phase separation

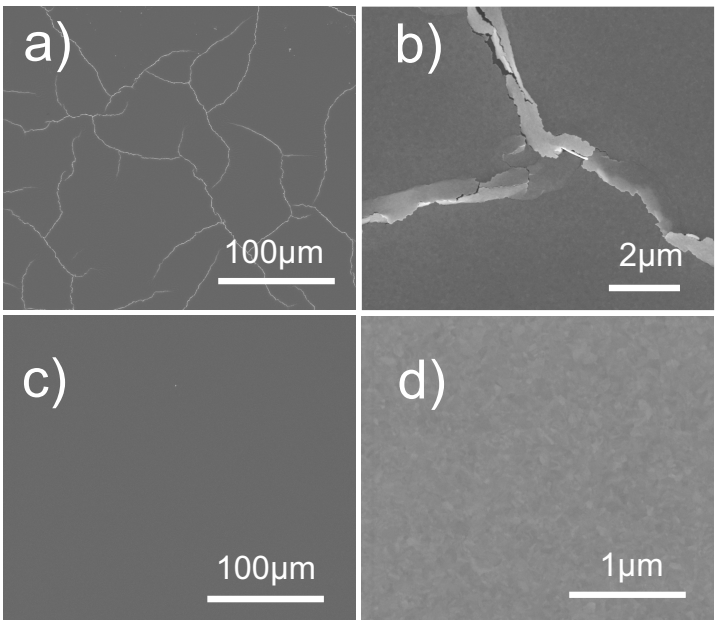

Figure 9: SEM images of the W capped stacks with 2 different compositions of the chalcogenide after anneal at 450°C. (a) 10%Si_9 and detail in (b), (c) 10%Si_10 and detail in (d).

and crystallization of the As, and subsequently crystallization of GeTe and As_2GeTe_4. The explanation for the composition being unaltered here is that the W capping layer for this composition remains intact up to at least 450°C, whereas for all other samples, cracking occurs (see SEM images in Figure 9). It is obvious that these cracks create a pathway for material loss and an intact capping layer prevents this.

In summary, the quaternary materials show no material loss up to 450°C, and hence have a better thermal stability compared to the ternaries. All quaternary SiGeAsTe compositions have a crystallization temperature above 450°C, and hence these films are compatible with BEOL temperatures. However, in combination with a W cap, only $As_{50}Te_{20}Ge_{20}Si_{10}$ does not show any degradation of the surface morphology up to 450°C. Hence this stack is BEOL compatible and is selected for integration to test its OTS performance. Note that other electrode materials may enable the integration of the other chalcogenide compositions as well, if they preserve a good surface morphology.

4.2. Ovonic threshold switching (OTS)

To verify the functionality of $As_{50}Te_{20}Ge_{20}Si_{10}$ as OTS material, a 20 nm thin chalcogenide film with 30 nm W electrode was integrated in mushroom type device structures. A cross section of the device is shown as an inset in Figure 10a.

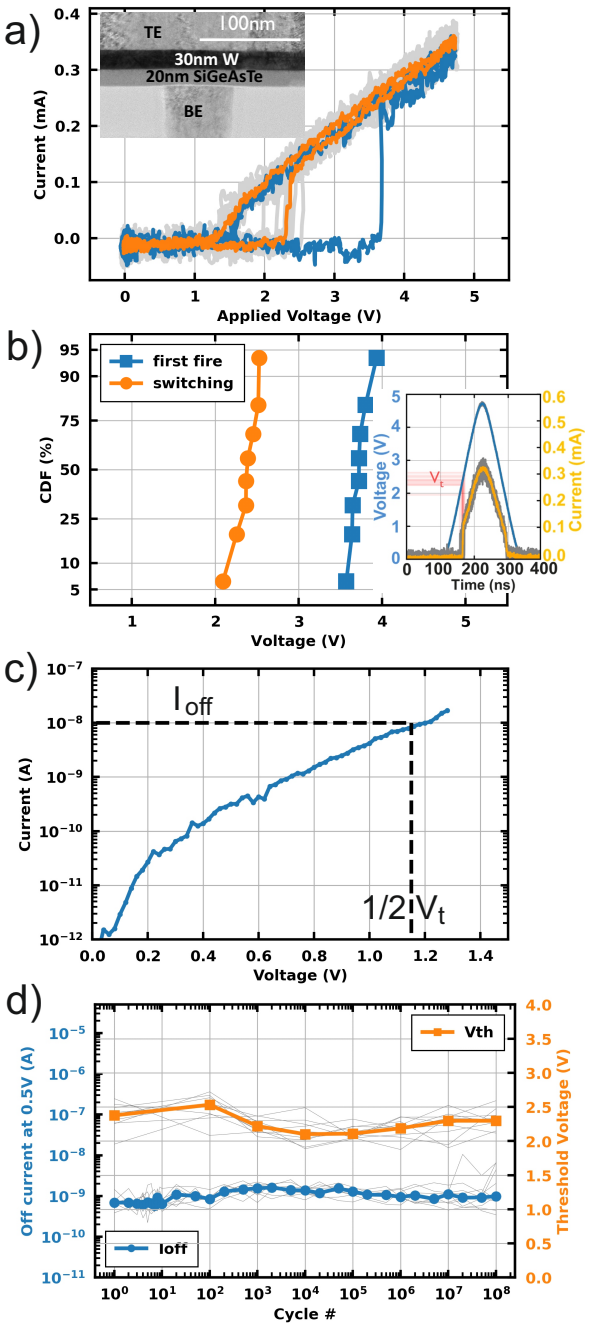

Figure 10: (a) IV curves showing the first cycle with higher threshold voltage (V_{ff}), and subsequent cycles with lower V_t. The orange curve gives the median. The inset shows a cross section of the device. (b) Cumulative distribution of V_{FF} and V_t. The inset shows the AC voltage pulse and current measurements. The extracted threshold voltages are indicated (c) DC IV curve after first fire to measure the leakage current. The current at 1/2 V_t is indicated. (d) Endurance measurement, showing V_t and I_{OFF} of 10 devices (grey) and the median curve over 10^8 cycles.

The devices are characterized in AC mode, by using a 5 V triangular pulse with 100 ns rise and fall time. The current was limited to $\sim 500\,\mu$A by an on-chip series resistance of 7 kΩ. The current flowing through the OTS device was extracted by measuring the voltage drop on a 50 Ω series resistor with an oscilloscope. The threshold voltage was extracted as the applied voltage where the largest variation in the OTS current (peak of the derivative) occurred. Figure 10a shows the typical IV curves, measured in positive polarity (i.e. positive bias applied on the top electrode). The material shows the typical IV behavior of an OTS material [8]. Below a threshold voltage V_t, the material is not conducting, and starts to conduct above it. When lowering the voltage again, the material drops back to a high resistive state below a holding voltage V_H. The first switching cycle shows a higher threshold voltage (*first fire* voltage, V_{FF}) compared to the subsequent cycles [37]. The cumulative distribution of V_{FF} and V_t for 8 devices is shown in Figure 10b, showing a median value of 3.8 V and 2.3 V for V_{FF} and V_t respectively. The inset of Figure 10b shows the AC measurements and the extraction of the threshold voltage. Note that mainly the first fire voltage here may be slightly impacted by the presence of an interfacial oxide layer on the TiN plugs because of the lack of a preclean step prior to chalcogenide deposition. The material supports a current density of more than 15 MA/cm^2 (the current density was limited here by the on chip resistance). For use as selector in cross bar arrays, another important parameter is the leakage current at half the threshold voltage, because non-addressed cells may see 1/2 V_t when a neighboring cell is selected. For our devices, the off current at 1.15 V (i.e. 1/2 V_t) is 10 nA (see Figure 10c). The endurance was measured, using the same pulse conditions on 75 nm devices and with the current limited to 400 μA. The off current is measured at 0.5 V and plotted, together with the threshold voltage as a function of the cycle number in Figure 10d. Over 10^8 cycles are achieved, without large drift in I_{OFF} or V_t, demonstrating an excellent endurance behavior.

4.3. Electronic structure of the material

The threshold switching phenomenon is generally well described as an electronic switching mechanism. These chalcogenide glasses are typically amorphous semiconductors, having a mobility gap E_g, and electronic trap states in the gap. Upon applying a critical electric field (at threshold voltage V_t) these traps get charged, changing their position with respect to the valence or conduction band edge, their dynamic charges increase [43] and therefore increasing the electrical conductivity of the material. The trap states can have different origins, depending on the material and the composition, but in general can be of valence alternation pairs nature, lone-pairs (from chalcogens or pnictogens) or mis-coordinated Ge nature (Ge-rich chalcogenides) [26]. Similar to what was shown for the Ge-Se chalcogenides [23, 26], we performed ab initio investigations of the electronic structure of $As_{50}Te_{20}Ge_{20}Si_{10}$, to probe for the presence of these electronic properties that can sustain OTS. A set of 10 different atomic models of 2x2x2 nm^3 have been generated as described in [26]. Figure 11a shows the density of states (DOS) near the mobility gap, aligned at

the valence edge. The mobility gap is rich in localized states of the amorphous phase (valence/conduction tails, mid-gap states) and the statistical box plots for traps and mobility gaps are shown in Figure 11b. The inverse participation ratio (IPR) was used to identify the localized states in the mobility edges of the atomic models. The trap states in the box plots are extracted from the raw DOS curves (shown in Figure 11a) and represent the deepest traps of these atomic models with respect to conduction or valence band for electron or hole trap states respectively. The valence edge is defined as the state which is lowest in energy and empty, whereas the conduction edge is the highest in energy and filled with electrons with an IPR equal to the median IPR value of the distribution of the valence band states. The mobility gaps for the different models is just the difference in energy between the valence and conduction edges. Figure 11c, shows the DOS, the IPR and the valence and conduction edges for one of the atomic models. For the nature of the traps, the valence tail states are predominantly Te 4p, the mid-gap states can be described as As 4p lone pair (LP), whereas the electronic traps near the conduction edge are of Ge- and SiAs3 nature, or σ^* antibonding combination of p states of Ge, As and Te. This is shown as insets for one of the atomic models in Figure 11c. The ensemble of overlapped DOS with their localized states (state localization lengths <2 nm) can already give an impression of the electronic structure inhomogeneity in a larger volume of the amorphous material. In conclusion, the electronic structure of the selected material shows a typical semiconducting mobility gap with localized states in the mobility gap that are essential for the OTS mechanism.

5. Conclusions

We used a combinatorial approach to create a large library of ternary Ge-As-Te and quaternary Si-Ge-As-Te thin films with different compositions. The thermal stability was investigated by means of *in situ* XRD to determine the crystallization temperature and XRF to detect material loss. The ternary alloys were more prone to material loss at 450°C, whereas this improved by adding Si. An optimum is achieved for 5 at% Si. For 10 at% Si, the As-rich films become more prone to As loss at higher temperatures. We explain this by Si segregation, leading to the presence of more pure As that is prone to sublimation. An optimal chalcogenide composition, being $As_{50}Te_{20}Ge_{20}Si_{10}$, with W electrode was identified as a BEOL compatible stack. Up to 450°C no crystallization nor material loss occurred, and the stack maintained a good surface morphology. The functionality of the material as OTS selector was demonstrated in 65 nm CD mushroom type devices. A high endurance of 10^8 cycles is obtained, with nearly no degradation in threshold voltage or off current.

Acknowledgements

The authors acknowledge the people from the imec 300 mm p-line for process support.

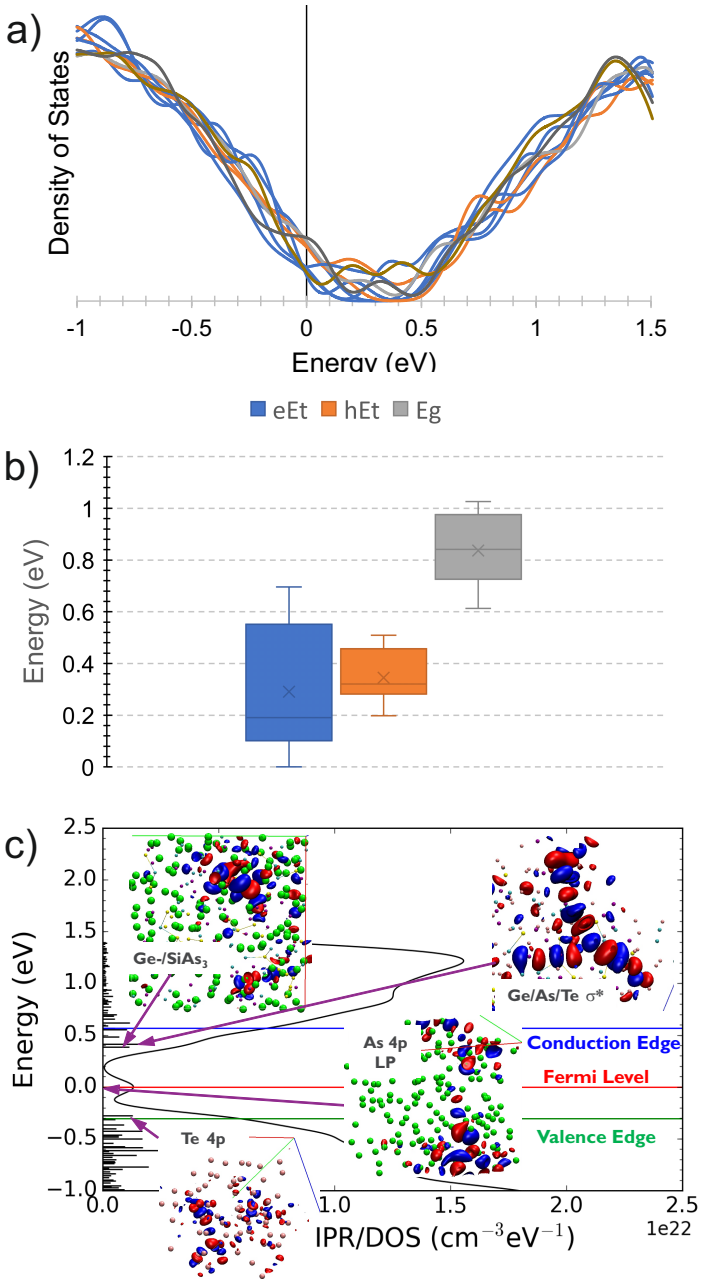

Figure 11: (a) Density of states for 10 amorphous SiGeAsTe models, aligned at the top of the valence edge (Gaussian smoothening kernel with $\sigma = 0.1\,\text{eV}$ applied). (b) Box plots of the electron (eEt wrt conduction edge), hole (hEt wrt to valence edge) trap states and the mobility gap (Eg). (c) DOS of one of the atomic models and identification of valence and conduction edge. The horizontal bars at the left represent the IPR of that state. The insets illustrate the state composition of the localized gap states. Red/blue isosurfaces represent the positive/negative lobes of the atomic orbitals for $> 99.9\,\%$ electronic density. Green/pink/yellow circles are representing various atomic sites in the atomic model.

Supporting information available

Table S1: Overview of the composition studied in this work, and the measured values. Table S2: Bond energies of the homonuclear and heteronuclear bonds that can be formed in the (Si-)Ge-As-Te system.

References

[1] N. M. Ravindra, W. Tang, S. Rassay, Transition metal dichalcogenides properties and applications, in: M. I. Pech-Canul, N. M. Ravindra (Eds.), Semiconductors: Synthesis, Properties and Applications, Springer International Publishing, Cham, 2019, pp. 333–396. doi:10.1007/978-3-030-02171-9_6.

[2] Y. Zhang, Y. Wang, J. Zhang, L. Xi, P. Zhang, W. Zhang, Pinning down high-performance cu-chalcogenides as thin-film solar cell absorbers: A successive screening approach, The Journal of Chemical Physics 144 (19) (2016) 194706. doi:10.1063/1.4950818.

[3] B. J. Eggleton, B. Luther-Davies, K. Richardson, Chalcogenide photonics, Nature Photonics 5 (3) (2011) 141. doi:10.1038/nphoton.2011.309.

[4] C. D. Wright, H. Bhaskaran, W. H. Pernice, Integrated phase-change photonic devices and systems, MRS Bulletin 44 (9) (2019) 721. doi:10.1557/mrs.2019.203.

[5] M. Zhu, K. Ren, Z. Song, Ovonic threshold switching selectors for three-dimensional stackable phase-change memory, MRS Bulletin 44 (9) (2019) 715. doi:10.1557/mrs.2019.206.

[6] D. Lencer, M. Salinga, M. Wuttig, Design rules for phase-change materials in data storage applications, Adv. Mater. 23 (18) (2011) 2030–2058. doi:10.1002/adma.201004255.

[7] G. W. Burr, R. S. Shenoy, K. Virwani, P. Narayanan, A. Padilla, B. Kurdi, H. Hwang, Access devices for 3d crosspoint memory, Journal of Vacuum Science & Technology B 32 (4) (2014). doi:10.1116/1.4889999.

[8] S. R. Ovshinsky, Reversible electrical switching phenomena in disordered structures, Phys. Rev. Lett. 21 (1968) 1450–1453. doi:10.1103/PhysRevLett.21.1450.

[9] Y. Koo, K. Baek, H. Hwang, Te-based amorphous binary ots device with excellent selector characteristics for x-point memory applications, in: 2016 IEEE Symposium on VLSI Technology, 2016, pp. 1–2. doi:10.1109/VLSIT.2016.7573389.

[10] Y. Koo, S. Lee, S. Park, M. Yang, H. Hwang, Simple binary ovonic threshold switching material site and its excellent selector performance for high-density memory array application, IEEE Electron Device Letters 38 (5) (2017) 568–571. doi:10.1109/LED.2017.2685435.

[11] M. Anbarasu, M. Wimmer, G. Bruns, M. Salinga, M. Wuttig, Nanosecond threshold switching of gete6 cells and their potential as selector devices, Applied Physics Letters 100 (14) (2012). doi:10.1063/1.3700743.

[12] Y. Koo, H. Hwang, Zn1-xtex ovonic threshold switching device performance and its correlation to material parameters, Scientific Reports 8 (12 2018). doi:10.1038/s41598-018-30207-0.

[13] B. Govoreanu, G. L. Donadio, K. Opsomer, W. Devulder, V. V. Afanas'ev, T. Witters, S. Clima, N. S. Avasarala, A. Redolfi, S. Kundu, O. Richard, D. Tsvetanova, G. Pourtois, C. Detavemier, L. Goux, G. S. Kar, Thermally stable integrated se-based ots selectors with >20 ma/cm2 current drive, $> 10^3$ half-bias nonlinearity, tunable threshold voltage and excellent endurance, in: 2017 Symposium on VLSI Technology, 2017, pp. T92–T93. doi:10.23919/VLSIT.2017.7998207.

[14] N. S. Avasarala, G. L. Donadio, T. Witters, K. Opsomer, B. Govoreanu, A. Fantini, S. Clima, H. Oh, S. Kundu, W. Devulder, M. H. van der Veen, J. V. Houdt, M. Heyns, L. Goux, G. S. Kar, Half-threshold bias ioffreduction down to na range of thermally and electrically stable high-performance integrated ots selector, obtained by se enrichment and n-doping of thin gese layers, in: 2018 IEEE Symposium on VLSI Technology, 2018, pp. 209–210. doi:10.1109/VLSIT.2018.8510680.

[15] J. Ho Lee, G. Hwan Kim, Y. Bae Ahn, J. Woon Park, S. Wook Ryu, C. Seong Hwang, H. Joon Kim, Threshold switching in si-as-te thin film for the selector device of crossbar resistive memory, Applied Physics Letters 100 (12) (2012). doi:10.1063/1.3696077.

[16] S. Kim, H.-D. Kim, S.-J. Choi, Intrinsic threshold switching responses in astesi thin film, Journal of Alloys and Compounds 667 (2016) 91 – 95. doi:10.1016/j.jallcom.2016.01.146.

[17] M.-J. Lee, D. Lee, H. Kim, H.-S. Choi, J.-B. Park, H. G. Kim, Y.-K. Cha, U.-I. Chung, I.-K. Yoo, K. Kim, Highly-scalable threshold switching select device based on chaclogenide glasses for 3d nanoscaled memory arrays, in: Electron Devices Meeting (IEDM), 2012 IEEE International, 2012, pp. 2.6.1–2.6.3. doi:10.1109/IEDM.2012.6478966.

[18] M.-J. Lee, D. Lee, S.-H. Cho, J.-H. Hur, S.-M. Lee, D. H. Seo, D.-S. Kim, M.-S. Yang, S. Lee, E. Hwang, M. R. Uddin, H. Kim, U.-I. Chung, Y. Park, I.-K. Yoo, A plasma-treated chalcogenide switch device for stackable scalable 3d nanoscale memory, Nature Communications 4 (2013) 2629. doi:10.1038/ncomms3629.

[19] A. Verdy, G. Navarro, V. Sousa, P. Noe, M. Bernard, F. Fillot, G. Bourgeois, J. Garrione, L. Perniola, Improved electrical performance thanks to sb and n doping in se-rich gese-based ots selector devices, in: 2017 IEEE International Memory Workshop (IMW), 2017, pp. 1–4.

[20] N. S. Avasarala, B. Govoreanu, K. Opsomer, W. Devulder, S. Clima, C. Detavernier, M. van der Veen, J. V. Houdt, M. Henys, L. Goux, G. S. Kar, Doped gese materials for selector applications, in: 2017 47th European Solid-State Device Research Conference (ESSDERC), 2017, pp. 168–171. doi:10.1109/ESSDERC.2017.8066618.

[21] H. Y. Cheng, W. C. Chien, I. T. Kuo, E. K. Lai, Y. Zhu, J. L. Jordan-Sweet, A. Ray, F. Carta, F. M. Lee, P. H. Tseng, M. H. Lee, Y. Y. Lin, W. Kim, R. Bruce, C. W. Yeh, C. H. Yang, M. BrightSky, H. L. Lung, An ultra high endurance and thermally stable selector based on teasgesise chalcogenides compatible with beol ic integration for cross-point pcm, in: 2017 IEEE International Electron Devices Meeting (IEDM), 2017, pp. 2.2.1–2.2.4.

[22] A. Velea, K. Opsomer, W. Devulder, J. Dumortier, J. Fan, C. Detavernier, M. Jurczak, B. Govoreanu, Te-based chalcogenide materials for selector applications, Scientific Reports 7 (1) (2017) 8103. doi:10.1038/s41598-017-08251-z.

[23] S. Clima, B. Govoreanu, K. Opsomer, A. Velea, N. S. Avasarala, W. Devulder, I. Shlyakhov, G. L. Donadio, T. Witters, S. Kundu, L. Goux, V. Afanasiev, G. S. Kar, G. Pourtois, Atomistic investigation of the electronic structure, thermal properties and conduction defects in ge-rich gexse1-x materials for selector applications, in: 2017 IEEE International Electron Devices Meeting (IEDM), 2017, pp. 4.1.1–4.1.4. doi:10.1109/IEDM.2017.8268323.

[24] G. Rampelberg, B. De Schutter, W. Devulder, K. Martens, I. Radu, C. Detavernier, In situ x-ray diffraction study of the controlled oxidation and reduction in the v-o system for the synthesis of vo2 and v2o3 thin films, J. Mater. Chem. C 3 (2015) 11357–11365. doi:10.1039/C5TC02553B.

[25] W. Devulder, K. Opsomer, J. Meersschaut, D. Deduytsche, M. Jurczak, L. Goux, C. Detavernier, Combinatorial study of ag-te thin films and their application as cation supply layer in cbram cells, ACS Combinatorial Science 17 (5) (2015) 334–340, pMID: 25860668. arXiv:https://doi.org/10.1021/acscombsci.5b00025, doi:10.1021/acscombsci.5b00025.

[26] S. Clima, D. Garbin, K. Opsomer, N. S. Avasarala, W. Devulder, I. Shlyakhov, J. Keukelier, G. L. Donadio, T. Witters, S. Kundu, B. Govoreanu, L. Goux, C. Detavernier, V. Afanas'ev, G. S. Kar, G. Pourtois, Ovonic threshold-switching gexsey chalcogenide materials: Stoichiometry, trap nature, and material relaxation from first principles, physica status solidi (RRL) - Rapid Research Letters 14 (5) 1900672. doi:10.1002/pssr.201900672.

[27] J. Hutter, M. Iannuzzi, F. Schiffmann, J. VandeVondele, cp2k: atomistic simulations of condensed matter systems, WIREs Computational Molecular Science 4 (1) (2014) 15–25. doi:10.1002/wcms.1159.

[28] As-ge-te vertical section of ternary phase diagram: Datasheet from "pauling file multinaries edition – 2012" in springermaterials (https://materials.springer.com/isp/phase-diagram/docs/c_0977000), copyright 2016 Springer-Verlag Berlin Heidelberg & Material Phases Data System (MPDS), Switzerland & National Institute for Materials Science (NIMS), Japan.

[29] As-ge-te vertical section of ternary phase diagram: Datasheet from "pauling file multinaries edition – 2012" in springermaterials (https://materials.springer.com/isp/phase-diagram/docs/c_0976999), copyright 2016 Springer-Verlag Berlin Heidelberg & Material Phases Data System (MPDS), Switzerland & National Institute for Materials Science (NIMS), Japan.

[30] As-ge-te vertical section of ternary phase diagram: Datasheet from "pauling file multinaries edition – 2012" in springermaterials (https://materials.springer.com/isp/phase-diagram/docs/c_0976996), copyright 2016 Springer-Verlag Berlin Heidelberg & Material Phases Data System (MPDS), Switzerland & National Institute for Materials Science (NIMS), Japan.

[31] As-ge-te vertical section of ternary phase diagram: Datasheet from "pauling file multinaries edition – 2012" in springermaterials (https://materials.springer.com/isp/phase-diagram/docs/c_0976997), copyright 2016 Springer-Verlag Berlin Heidelberg & Material Phases Data System (MPDS), Switzerland & National Institute for Materials Science (NIMS), Japan.

[32] As-ge-te vertical section of ternary phase diagram: Datasheet from "pauling file multinaries edition – 2012" in springermaterials (https://materials.springer.com/isp/phase-diagram/docs/c_0976998), copyright 2016 Springer-Verlag Berlin Heidelberg & Material Phases Data System (MPDS), Switzerland & National Institute for Materials Science (NIMS), Japan.

[33] G. Ghosh, Materials Science International Team, MSIT, As-ge-te ternary phase diagram evaluation · phase diagrams, crystallographic and thermodynamic data: Datasheet from msi eureka in springermaterials (https://materials.springer.com/msi/docs/sm_msi_r_10_014890_01), copyright 1994 MSI Materials Science International Services GmbH.

[34] M. Lankhorst, Modelling glass transition temperatures of chalcogenide glasses. applied to phase-change optical recording materials, J. Non-Cryst. Solids 297 (2-3) (2002) 210 – 219. doi:10.1016/S0022-3093(01)01034-1.

[35] S. Raoux, M. Salinga, J. L. Jordan-Sweet, A. Kellock, Effect of al and cu doping on the crystallization properties of the phase change materials sbte and gesb, J. Appl. Phys. 101 (4) (2007) 044909. doi:10.1063/1.2654556.

[36] D. Lencer, M. Salinga, B. Grabowski, T. Hickel, J. Neugebauer, M. Wuttig, A map for phase-change materials, Nat Mater 7 (12) (2008) 972–977. doi:10.1038/nmat2330.

[37] J. Bosnell, C. Thomas, Preswitching electrical properties, 'forming' and switching in amorphous chalcogenide alloy threshold and memory devices, Solid-State Electronics 15 (11) (1972) 1261 – 1271. doi:10.1016/0038-1101(72)90047-0.

[38] K. Homma, H. Henisch, S. Ovshinsky, New experiments on threshold switching in chalcogenide and non-chalcogenide alloys, Journal of Non-Crystalline Solids (1980) 1105 – 1110doi:10.1016/0022-3093(80)90347-6.

[39] International Centre for Diffraction Data, Newtown Square, PA, JCPDS Data Card no. 00-005-0632 (2004).

[40] International Centre for Diffraction Data, Newtown Square, PA, JCPDS Data Card no. 00-043-1330 (2004).

[41] International Centre for Diffraction Data, Newtown Square, PA, JCPDS Data Card no. 00-022-0312 (2004).

[42] International Centre for Diffraction Data, Newtown Square, PA, JCPDS Data Card no. 00-047-1079 (2004).

[43] J.-Y. Raty, P. Noe, Ovonic threshold switching in se-rich gexse1-x glasses from an atomistic point of view: The crucial role of the metavalent bonding mechanism, physica status solidi (RRL) - Rapid Research Letters 14 (5) (2020) 1900581. doi:10.1002/pssr.201900581.